Supplemental Proceedings: Volume 2: Materials Characterization, Computation and Modeling
TMS (The Minerals, Metals & Materials Society), 2009

Coarsening of 3D Thin Films under the Influence of Strong Surface Anisotropy, Elastic Stresses

Peng Zhou[1], Steven Wise[2] and John Lowengrub[1]

[1]Math Department, University of California, Irvine,
Irvine, CA 92697 USA
[2]Math Department, University of Tennessee, Knoxville,
Knoxville, TN 37996-1300 USA

Keywords: Thin film, Strong surface anisotropy, Elastic strains

Abstract

We develop a diffuse interface model to investigate the three dimensional coarsening in thin films. In this model, both strong surface anisotropy with linear Willmore regularization, elastic stresses and deposition are included. The governing equation for the phase field parameter is a sixth order Cahn-Hilliard Equation due to the presence of surface anisotropy and the linear Willmore regularization. The simulated system is assumed to be in mechanical equilibrium with misfit in the film generated by lattice mismatch in the substrate. Thus, the Cauchy-Navier equations are solved for elastic displacements which lead to the elastic energy. Both the Cahn-Hilliard equation and the Cauchy-Navier equations are solved with an non-stiff, adaptive nonlinear multigrid method. Simulation results of coarsening in three dimensions with different strengths of the surface anisotropy, misfit strain, and deposition rates are shown. Comparison and analysis of these results help to explain their influence on coarsening processes in thin films.

Introduction

It is known that both surface anisotropy and elastic strains have an important influence on the morphological evolution of thin films. The effects of strong surface anisotropy have been studied in great detail in the problem of crystal growth[1]. In the case of an isotropic surface energy, a crystal usually shows a spherical shape with all crystal orientations present. In contrast, strong surface anisotropies result in missing crystal orientations and enable formation of facets at the surface[2]. However, non-convexity of this strong surface anisotropy energy leads to ill-posedness of the Cahn-Hilliard equation[3][4]. Hence, Willmore regularization has been proposed to resolve this issue by smoothing out the transitions near the sharp corners at the corrugated surface[5].

Besides surface anisotropy, elastic strains also play an important role in the morphological evolution of thin films. Due to the difference in crystal structures between the substrate and film, misfit strains arise. The elastic energy stored in the thin films owing to these misfit strains can be relieved by developing pits, islands and quantum fortresses[6]. Formation of these structures increase the free surface area to aid the relaxation of elastic energy, though at the cost of increasing the surface free energy[7]. Competition between the elastic energy and the surface free energy, combined with deposition of materials at the surface dominate the process of morphological evolution of thin films.

In this paper, a diffuse interface model is used to study the coarsening of thin films in three dimensions with different strengths of the surface anisotropy, misfit strains, and deposition rates. Formulation of governing equations is presented in section 2. Numerical methods

Report Documentation Page

Form Approved
OMB No. 0704-0188

1. REPORT DATE	2. REPORT TYPE	3. DATES COVERED
FEB 2011		**00-00-2011 to 00-00-2011**

4. TITLE AND SUBTITLE
Coarsening of 3D Thin Films under the Influence of Strong Surface Anisotropy, Elastic Stresses

5a. CONTRACT NUMBER
5b. GRANT NUMBER
5c. PROGRAM ELEMENT NUMBER

6. AUTHOR(S)

5d. PROJECT NUMBER
5e. TASK NUMBER
5f. WORK UNIT NUMBER

7. PERFORMING ORGANIZATION NAME(S) AND ADDRESS(ES)
University of California,Math Department,Irvine,CA,92697

8. PERFORMING ORGANIZATION REPORT NUMBER

9. SPONSORING/MONITORING AGENCY NAME(S) AND ADDRESS(ES)

10. SPONSOR/MONITOR’S ACRONYM(S)

11. SPONSOR/MONITOR’S REPORT NUMBER(S)

12. DISTRIBUTION/AVAILABILITY STATEMENT
Approved for public release; distribution unlimited

13. SUPPLEMENTARY NOTES
See also ADM002300. Presented at the Minerals, Metals and Materials Annual Meeting and Exhibition (138th)(TMS 2009) Held in San Francisco, California on February 15-19, 2009. Sponsored in part by the Navy. U.S. Government or Federal Purpose Rights.

14. ABSTRACT
We develop a di use interface model to investigate the three dimensional coarsening in thin lms. In this model, both strong surface anisotropy with linear Willmore regularization elastic stresses and deposition are included. The governing equation for the phase eld parameter is a sixth order Cahn-Hilliard Equation due to the presence of surface anisotropy and the linear Willmore regularization. The simulated system is assumed to be in mechanical equilibrium with mis t in the lm generated by lattice mismatch in the substrate. Thus the Cauchy-Navier equations are solved for elastic displacements which lead to the elastic energy. Both the Cahn-Hilliard equation and the Cauchy-Navier equations are solved with an non-sti , adaptive nonlinear multigrid method. Simulation results of coarsening in three dimensions with di erent strengths of the surface anisotropy, mis t strain, and deposition rates are shown. Comparison and analysis of these results help to explain their in uence on coarsening processes in thin lms.

15. SUBJECT TERMS

16. SECURITY CLASSIFICATION OF:			17. LIMITATION OF ABSTRACT	18. NUMBER OF PAGES	19a. NAME OF RESPONSIBLE PERSON
a. REPORT	b. ABSTRACT	c. THIS PAGE			
unclassified	**unclassified**	**unclassified**	**Same as Report (SAR)**	**8**	

Standard Form 298 (Rev. 8-98)
Prescribed by ANSI Std Z39-18

are given in section 3. Preliminary results with different strengths in surface anisotropy are presented and discussed in section 4.

Formulation

The thermodynamic system considered here consists of a thin film phase and a vapor phase. A phase variable c is introduced such that $c = 0.0$ is the vapor phase and $c = 1.0$ is the thin film phase. Both strong surface anisotropy and linear Willmore regularization have been introduced to the model to give the surface a corrugated morphology with smooth corners. Elastic stresses arise from the misfit strains are also included.

Thus the total free energy of this system is given by:

$$
\begin{aligned}
E &= \int_\Omega \frac{1}{\epsilon}\gamma(\mathbf{n})(f(c) + \frac{\epsilon^2}{2}|\nabla c|^2)d\vec{X} \\
&+ \frac{\beta}{2\epsilon^3}\int_\Omega (-\epsilon^2\Delta c)^2 d\vec{X} \\
&+ \int_\Omega W(c,E)d\vec{X},
\end{aligned} \tag{1}
$$

where

$$f(c) = \frac{1}{4}Ac^2(1-c)^2. \tag{2}$$

$f(c)$ is a double well chemical free energy density with $c = 0.0$ and $c = 1.0$ being the two minima, and A is a parameter related to the height of the energy barrier; $\frac{\epsilon^2}{2}|\nabla c|^2$ is the gradient energy density which takes into account the non-local interactions due to the phase field variation across the interface;

$$\gamma(\mathbf{n}) = 1 + \alpha\Gamma(\mathbf{n}), \tag{3}$$

$$\Gamma(\mathbf{n}) = 4\sum_{i=1}^{d} n_i^4 - 3, \qquad d = 2,3 \tag{4}$$

$$\mathbf{n} = \frac{\nabla c}{|\nabla c|}. \tag{5}$$

where $\gamma(\mathbf{n})$ is the function of surface anisotropy with $\mathbf{n}$ being the normal vector at the interface; α is dimensionless and defines the strength of the anisotropy, and $\Gamma(\mathbf{n})$ as given in Equation (2) indicates that the anisotropy is four-fold symmetric with n_i being each component of the normal vector $\mathbf{n}$. As shown in equation (1), the anisotropy surface energy $\gamma(\mathbf{n})$ times both the chemical free energy denstiy and the gradient energy density. It has been shown in [8] that the thickness of interfaces from this new formulation is uniform and independent of the crystal orientation.

The second term given in Equation (1) is the linear Willmore regularization term and β is regularization parameter. The sharp corners due to formation of facets will be smoothed out due to the higher-order derivative in this term. The last term $W(c,E)$ is the elastic energy given by,

$$W(c,E) = \frac{1}{2}\sum_{i,j=1}^{d} T_{ij}(E_{ij} - \delta_{ij}e(c)). \tag{6}$$

Accordingly, we define

$$
\begin{aligned}
T_{ij} &= \sum_{i,j=1}^{d} C_{ijkl}(c)(E_{kl} - \delta_{kl} e(c)), && (7)\\
E_{kl} &= \frac{1}{2}(u_{i,j} + u_{j,i}), && (8)\\
e(c) &= \eta q(c); q(c) = c^2(3-2c), && (9)\\
C_{ijkl} &= C^0_{ijkl} + q(c)(C^1_{ijkl} - C^0_{ijkl}), && (10)
\end{aligned}
$$

where T_{ij} and E_{ij} are linear stress and strain tensor related by Hooke's Law as given in Equation (7); $\mathbf{u}$ are elastic displacements; $e(c)$ is the misfit strain arising from the mismatch of crystal lattice with the magnitude given by η; the cubic elastic stiffness tensor C_{ijkl} is defined to be an interpolation of the stiffness tensors, C^0_{ijkl} and C^1_{ijkl}, of the two phases weighted by $q(c)$. For the vapor phase, C^0_{ijkl} are assigned with values three orders of magnitude lower than those of the film phase.

Evolution of the phase field is determined by the sixth-order regularized, anisotropic Cahn-Hilliard equation as shown below,

$$
\begin{aligned}
\frac{\partial c}{\partial \tau} &= \nabla \cdot (M(c)\nabla\mu) + S(c, \mathbf{n}), && (11)\\
\mu &= \gamma(\mathbf{n}) f'(c) - \epsilon^2 \nabla \cdot (\nabla c + \nabla A(\mathbf{n})\nabla c) - \beta\Delta\nu + W'(c, E), && (12)\\
\nu &= \epsilon^2 \Delta c, && (13)
\end{aligned}
$$

where the generalized chemical potential μ is the variational derivative of the total free energy density; $M(c)$ is the surface mobility given by $M_0 c(1-c)$ with M_0 being the mobility coefficient; $S(c, \mathbf{n}) = V_d Q R c^2 (1-c)^2 n_3$ is the deposition term localized at the film-vapor interface[9] with V_d being the deposition rate, Q is a scale factor to match the sharp interface result, and R is a random number$(0.9 \leq R \leq 1.1)$. For computational convenience, the Cahn-Hilliard equation is split into three second-order equations with c, μ and ν being the three dependent variables.

Elastically, the film phase and the vapor phase are assumed to be in mechanical equilibrium. The conditions of mechanical equilibrium are used to determine the elastic fields.

$$
\sum_{j=1}^{d} T_{ij,j} = 0, \qquad\qquad d = 2, 3. \tag{14}
$$

This quasi-stationary assumption combined with stresses and strains given in Equation (7) lead to the Carchy-Navier equations for elastic displacements. Elastic energy is determined via Equation (6) once the displacements are found from these Carchy-Navier equations.

For these governing equations, periodic boundary conditions are used in the horizontal directions for each dependent variable. Neumann boundary conditions are used for the Cahn-Hillard equations in the vertical direction of the computational cell; Traction-free boundary conditions and Dirichlet boundary conditions are used for the displacements at the top and bottom of the computational cell, respectively.

<u>Nondimensionalization</u>

All governing equations are nondimensionalized for computational convenience. The scaled position and scaled time are defined to be $\vec{x} = \frac{\vec{X}}{L}$ and $t = \frac{\tau}{T}$ where the characteristic Length

L is chosen to be $20nm$ and the characteristic time T is given as below:

$$T = \frac{L^2}{M_0 A}, \tag{15}$$

The chemical free energy density is normalized by the parameter A, and $M(c)$ by M_0. The stiffness coefficients are normalized by C^1_{44}. The misfit strain and the elastic energy density are normalized by η and $\eta^2 C^1_{44}$, which are usually used as the characteristic scales for the elastic energy[9]. Other non-dimensional quantities characterizing this physical system are listed below,

$$\bar{\epsilon} = \frac{\epsilon}{L\sqrt{A}}; \bar{\beta} = \frac{\beta}{L^2}; \bar{V}_d = \frac{V_d L^2}{M_0 A}; Z = \frac{\eta^2 C^1_{44}}{A} \tag{16}$$

where Z is a parameter relating to the strength of the elastic effects. Most of the nondimensionalized quantities are denoted with an over bar correspondingly. The non-dimensional governing equations can be derived by equating the operators and sources shown by equations (20)-(24) and (25)-(29) in the next subsection, respectively.

The physical values for the characteristic length and time, and the calculated values for the normalized quantities except those for the deposition term are listed in Table 1.

paramter	L	T	$\bar{\epsilon}$	$\bar{\beta}$	Z
value	20(nm)	10-100(s)	2.4×10^{-2}	0.01	0.125-0.25

Table 1: *Physical values and calculated values used in simulation*

Numerical methods

The governing equations given in equations (11) and (14) are solved by adaptive nonlinear multigrid methods developed by Wise, Kim and Lowengrub[4]. Briefly, the sixth order Cahn-Hilliard equation with linear Willmore regularization is split into three second order equations as shown in equation (11). These three equations and the elastic Cauchy-Navier equations are solved simultaneously using an adaptive multilevel multigrid method to determine the profile of the composition field c and the displacement field $\mathbf{u}$. Second order center finite differences are used for the spatial discretization and a gradient stable scheme is adopted for the time discretization.

For the gradient stable scheme, the normalized chemical free energy density is split into a contractive term and an expansive term as shown below,

$$\begin{aligned} \bar{f}(c) &= \bar{f}_c(c) - \bar{f}_e(c), && (17)\\ \bar{f}_c(c) &= \frac{1}{4}(c - \frac{1}{2})^4 + \frac{1}{64}, && (18)\\ \bar{f}_e(c) &= \frac{1}{8}(c - \frac{1}{2})^2. && (19) \end{aligned}$$

A full approximation scheme (FAS) multigrid method is applied to solve the nonlinear governing equations and self adaptive block-structured Cartesian mesh refinement is used to resolve narrow interfacial layers. For the FAS method, equations are split into operator (N) and source (S) terms[4] with the components of the operator being

$$\begin{aligned} N_1 &= c^{n+1} - dt\nabla \cdot \bar{M}(c^{n+1,k})\nabla\bar{\mu}^{n+1}, && (20)\\ N_2 &= \bar{\mu}^{n+1} - \bar{f}'_c(c^{n+1}) + nu^{n+1} - \beta\Delta\bar{\nu}^{n+1}, && (21) \end{aligned}$$

$$
\begin{aligned}
N_3 &= \bar{\nu}^{n+1} - \bar{\epsilon}^2 \Delta c^{n+1}, &(22)\\
N_4 &= \frac{\partial}{\partial x_1}\left(\bar{C}_{11}\frac{\partial u_1}{\partial x_1} + \bar{C}_{11}\frac{\partial u_2}{\partial x_2}\right) + \frac{\partial}{\partial x_2}\left(\bar{C}_{44}\frac{\partial u_1}{\partial x_2} + \bar{C}_{44}\frac{\partial u_2}{\partial x_1}\right), &(23)\\
N_5 &= \frac{\partial}{\partial x_2}\left(\bar{C}_{22}\frac{\partial u_2}{\partial x_2} + \bar{C}_{12}\frac{\partial u_1}{\partial x_1}\right) + \frac{\partial}{\partial x_1}\left(\bar{C}_{44}\frac{\partial u_2}{\partial x_1} + \bar{C}_{44}\frac{\partial u_1}{\partial x_2}\right), &(24)
\end{aligned}
$$

and those of source terms being

$$
\begin{aligned}
S_1 &= c^n + \bar{V}_d Q R (c^n)^2 (1-c^n)^2 n_z, &(25)\\
S_2 &= -\bar{f}_e'(c^n) + \alpha\Gamma(\mathbf{n})\bar{f}'(c^n) - \bar{\epsilon}^2 \nabla \cdot A(\mathbf{n})\nabla c^{n+1} + W'(c^{n+1}, E^{n+1}), &(26)\\
S_3 &= 0, &(27)\\
S_4 &= \frac{\partial}{\partial x_1}\left[(\bar{C}_{11} + \bar{C}_{12}) e(c^{n+1})\right], &(28)\\
S_5 &= \frac{\partial}{\partial x_2}\left[(\bar{C}_{22} + \bar{C}_{12}) e(c^{n+1})\right], &(29)
\end{aligned}
$$

The operator and source terms for the Cauchy-Navier equations are only shown in the 2D case. The 3D case is analogously defined. More details about the numerical method can be found in the work of Wise et al[4].

The size of the computational cell is set to be $6.4 \times 6.4 \times 3.2$. Two refinement levels are used and the root level is a grid of size $64 \times 64 \times 32$. Thus the finest mesh size is $h = 0.025$. The time step used in the simulation is 1.6×10^{-2}. The tolerance set for the convergence of the multigrid solver is 1.0×10^{-6}.

Compared with the Crank-Nicholson method for time discretization, the gradient stable method can allow a time step which is 16 times of that in the former case. In the 3D simulations presented below, the estimated execution time is successfully reduced from 8-10 months to about one month.

Preliminary Simulation Results

In this section, preliminary simulation results are shown that describe the influence of the strength of surface anisotropy without material deposition. Fig. 1 shows the morphological evolution of thin films with an initial sinusoidal perturbation which is given by,

$$c(x_1, x_2, x_3) = \frac{1}{2}\frac{1.0 - \tanh(x_3 - r(x_1, x_2))}{2\sqrt{2}\bar{\epsilon}} \tag{30}$$

where

$$r(x_1, x_2) = 1.6 + 0.06 sin(\frac{6\pi x_1}{6.4})\sin(\frac{6\pi x_2}{6.4}). \tag{31}$$

The magnitude of this sinusoidal perturbation is 0.06. The surface anisotropy parameter α is set to be $\alpha = 0.2$ in Fig. 1(a) and (b), and $\alpha = 0.3$ in (c) and (d), respectively. However, in both cases the strengths of the elasticity are the same with $Z = 0.25$. A comparison of Fig. 1(a) and (c), and (b) and (d) at the non-dimensional times $t = 1.6$ and $t = 6.4$, show that the pyramids formed in (c) and (d)present sharper corners and edges when the surface anisotropy is stronger. In Fig. 1(c), pits are also found to form at the top of the pyramids to help decrease the surface anisotropy energy.

Fig. 2 shows the morphological evolution of thin films with an initial random perturbation as given by equation (30) with $r(x_1, x_2)$ replaced by,

$$r(x_1, x_2) = 1.6 + 0.0001\zeta(x_1, x_2). \tag{32}$$

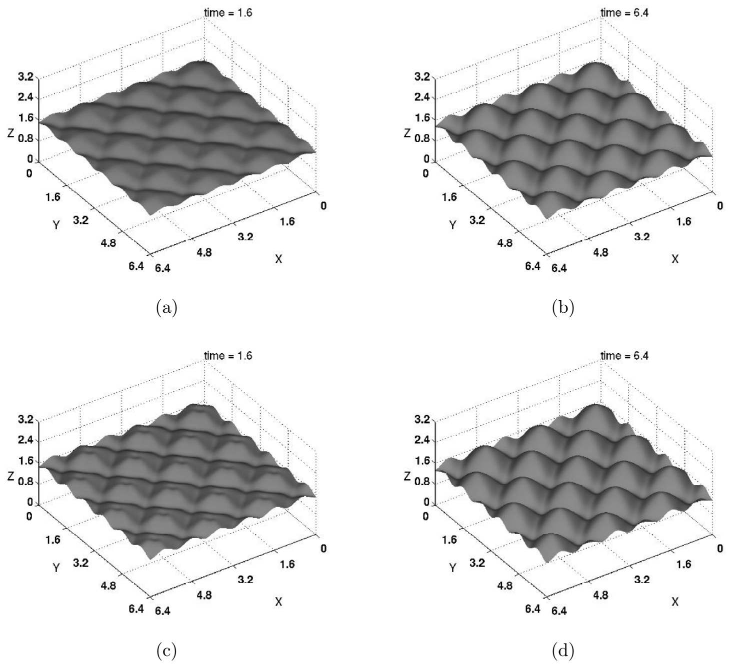

Figure 1: Morphological evolution of thin films with an initial sinusoidal perturbation, and $Z = 0.25$: (a) $\alpha = 0.2$, $t = 1.6$; (b) $\alpha = 0.2$, $t = 6.4$; (c) $\alpha = 0.3$, $t = 1.6$; (d) $\alpha = 0.3$, $t = 6.4$.

where $\zeta(x_1, x_2)$ is a random number and the magnitude of the perturbation is 10^{-4}. Other physical parameters are set to be the same as in the former case. Compared with those shown in Fig. 2(a) and (b), the morphological evolution in Fig. 2(c) and (d) proceeds much faster due to the stronger surface anisotropy. At time $t = 1.6$, the surface in Fig. 2(a) with $\alpha = 0.2$ is still close to being planar, while that in Fig. 2(c) has already become highly corrugated. The difference shown by these preliminary results suggests that at the early times, surface anisotropy is the dominant driving force for morphological evolution, since a corrugated surface can greatly lower the surface anisotropy energy initially.

In Fig. 3, longer-time simulation results with $\alpha = 0.2$ and $Z = 0.25$ are shown for both initial perturbations. Fig. 3(a) and (b) demonstrate well-developed domes and valleys for the surface of the thin film with a sinusoidal perturbation. As time evolves, the valleys are supposed to deepen to aid the relaxation of elastic stresses and strains, thus lower the total elastic energy. No coarsening seems to occur in these two plots since the domes are approximately the same size due to the initial perturbation. However, in Fig. 3(c) and (d), coarsening of the domes is observed. This process lowers the total elastic energy. Due to the use of the gradient stable method, the total execution time for these two longer-time simulations is about 2 weeks.

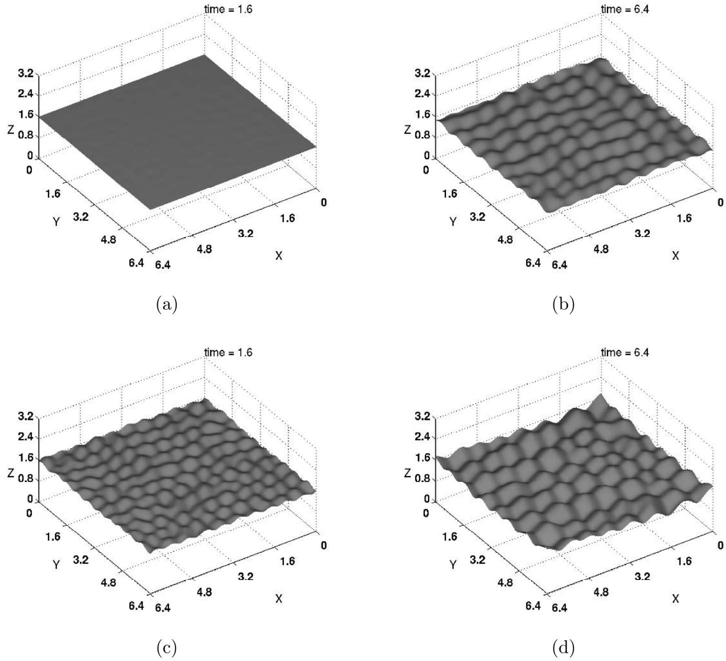

Figure 2: Morphological evolution of thin films with an initial random perturbation, and $Z = 0.25$: (a) $\alpha = 0.2$, $t = 1.6$; (b) $\alpha = 0.2$, $t = 6.4$; (c) $\alpha = 0.3$, $t = 1.6$; (d) $\alpha = 0.3$, $t = 6.4$.

Summary

In this paper, a diffuse interface model, including strong surface anisotropy with linear Willmore regularization, elastic stresses and deposition, is developed to simulate the three dimensional coarsening in thin films. The high-order governing equations, i.e, the Cahn-Hilliard equation and the Cauchy-Navier equations are solved with an non-stiff, adaptive nonlinear multigrid method. A gradient stable method is applied for the time discretization which significantly reduces the total execution time of the three dimensional simulations. Preliminary simulation results of coarsening in three dimensions with different strengths of the surface anisotropy suggests that surface anisotropy is the dominant driving force for morphological evolution initially since a corrugated surface can greatly lower the surface anisotropy energy. More simulation results will be provided in the future to further characterize the coarsening processes in thin films.

Acknowledgement

We gratefully acknowledge the financial support of the National Science Foundation, Division of Mathematical Sciences (DMS) and the Division of Materials Research (DMR).

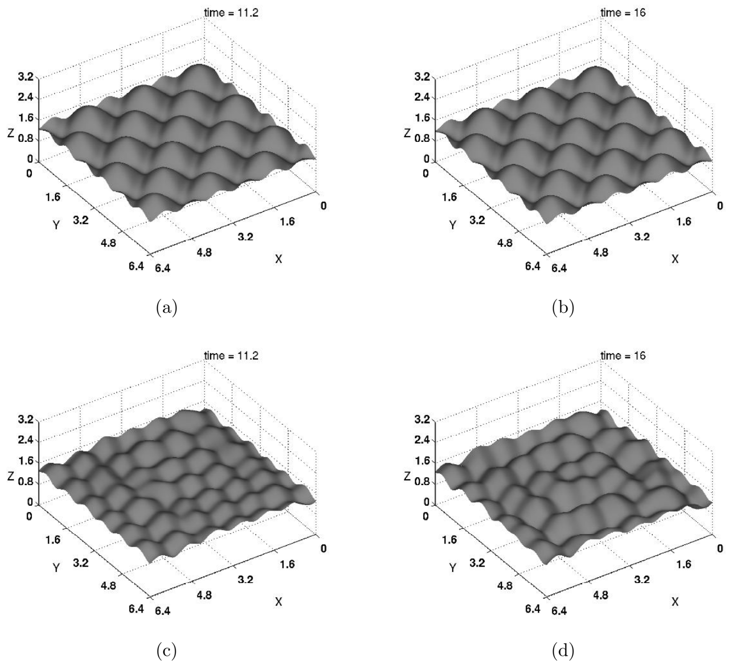

Figure 3: Longer-time morphological evolution of thin films with $\alpha = 0.2$, $Z = 0.25$: and with an initial sinusoidal perturbation (a) $t = 11.2$, (b) $t = 16$; and with an initial random perturbation (c) $t = 11.2$, (d) $t = 16$.

References

[1] Alberto Pimpinelli, Jacques Villain, Physics of crystal growth, Cambridge ; New York : Cambridge University Press, 1998

[2] Robert F. Sekerka, J. Crystal Growth. 275, 2005, 77-82

[3] M. Burger, F. Hauβer, C. St$\ddot{o}$cker, A. Voigt, J. Comput. Phys. 225, issue 1, July 2007, P183-205

[4] S. Wise, J. Kim, J. Lowengrub, J. Comput. Phys. 226, issue 1, Sept. 2007, P 414-446

[5] A. DiCarlo, M. Gurtin, P. Podio-Guidugli, SIAM J. Appl. Math 52(1992) 11111119

[6] J. Gray, R. Hull, J. Floro, Appl. Phys. Lett. 81(2002) 2445

[7] M. Grinfeld, Dokl. Akad. Nauk SSSR 265(1982) 836

[8] S. Torabi, S. Li, S. Wise, A. Voigt, J. Lowengrub, Proc. Roy. Soc. Lond. Sec. A, in review

[9] S. Wise, J. Lowengrub, J. Kim, W. Johnson, Superlattices and Microstructures 36(2004) 293-304